Active control of Alfvén eigenmodes in magnetically confined toroidal plasmas

OPEN ACCESS
IOP Publishing
Plasma Physics and Controlled Fusion
Plasma Phys. Control. Fusion **61** (2019) 054007 (12pp)
https://doi.org/10.1088/1361-6587/aaef08

Active control of Alfvén eigenmodes in magnetically confined toroidal plasmas

M Garcia-Munoz[1], S E Sharapov[2], M A Van Zeeland[3], E Ascasibar[4], A Cappa[4], L Chen[5,6], J Ferreira[7], J Galdon-Quiroga[1], B Geiger[8], J Gonzalez-Martin[1], W W Heidbrink[6], T Johnson[9], Ph Lauber[8], M Mantsinen[10,11], A V Melnikov[12,13,14], F Nabais[6], J F Rivero-Rodriguez[1], L Sanchis-Sanchez[1], P Schneider[8], J Stober[8], W Suttrop[8], Y Todo[15], P Vallejos[9], F Zonca[5,16] and the AUG and MST1 Teams[17]

[1] Dept. of Atomic, Molecular and Nuclear Physics, Universidad de Sevilla, Sevilla, Spain
[2] Culham Science Centre, Abingdon, United Kingdom
[3] General Atomics, San Diego, CA, United States of America
[4] CIEMAT, Madrid, Spain
[5] IFTS and Dept. of Physics, Zhejiang University, Hangzhou, People's Republic of China
[6] Dept. of Physics and Astronomy, University of California, Irvine, CA, United States of America
[7] IST, Lisbon, Portugal
[8] Max Planck Institut für Plasmaphysik, Garching, Germany
[9] VR/Royal Institute of Technology KTH, Sweden
[10] Barcelona Supercomputer Center, Barcelona, Spain
[11] ICREA, Pg. Lluís Companys 23, Barcelona, Spain
[12] National Research Centre 'Kurchatov Institute', 123182, Moscow, Russia
[13] National Research Nuclear University MEPhI, 115409, Moscow, Russia
[14] Moscow Institute of Physics and Technology, Dolgoprudny, Russia
[15] National Institute for Fusion Science, Toki, Japan
[16] ENEA, Fusion and Nuclear Safety Department, C. R. Frascati, Italy

E-mail: mgm@us.es

Received 14 July 2018, revised 14 October 2018
Accepted for publication 7 November 2018
Published 29 March 2019

Abstract

Alfvén waves are electromagnetic perturbations inherent to magnetized plasmas that can be driven unstable by a free energy associated with gradients in the energetic particles' distribution function. The energetic particles with velocities comparable to the Alfvén velocity may excite Alfvén instabilities via resonant wave–particle energy and momentum exchange. Burning plasmas with large population of fusion born super-Alfvénic alpha particles in magnetically confined fusion devices are prone to excite weakly-damped Alfvén eigenmodes (AEs) that, if allowed to grow unabated, can cause a degradation of fusion performance and loss of energetic ions through a secular radial transport. In order to control the fast-ion distribution and associated Alfvénic activity, the fusion community is currently searching for external actuators that can control AEs and energetic ions in the harsh environment of a fusion reactor. Most promising control techniques are based on (i) variable fast-ion sources to modify gradients in the energetic particles' distribution, (ii) localized electron cyclotron resonance heating to affect the fast-ion

[17] H Meyer *et al* 2017 *Nucl. Fusion* 57 102014.

slowing-down distribution, (iii) localized electron cyclotron current drive to modify the equilibrium magnetic helicity and thus the AE existence criteria and damping mechanisms, and (iv) externally applied 3D perturbative fields to manipulate the fast-ion distribution and thus the wave drive. Advanced simulations help to identify the key physics mechanisms underlying the observed AE mitigation and suppression and thus to develop robust control techniques towards future burning plasmas.

Keywords: Alfvén, perturbations, waves, MHD, fusion, stellarator, tokamak

(Some figures may appear in colour only in the online journal)

1. Introduction

In magnetically confined fusion devices, super-thermal particles must be well confined until they slow down to the plasma bulk [1]. Fusion born alpha particles as well as energetic particles produced by external heating systems such as neutral beam injectors (NBI) or ion cyclotron resonance heating (ICRH) are, however, a source of free energy that can destabilize a rich spectrum of magnetohydrodynamic (MHD) fluctuations. Alfvén waves [2] are electromagnetic perturbations inherent to a magnetized plasma that are often driven unstable by spatial gradients in a resonant energetic particle population. In present day tokamaks and stellarators, a net wave–particle energy and momentum exchange is always accompanied by a transport of energetic particles. A secular transport can end in a particle loss that, if it is not mitigated, can lead to a degradation of the reactor performance. An intense and localized energetic particle loss can even pose serious threats to the integrity of the plasma facing components and vacuum vessel. Indeed, in tokamaks, under unfavourable conditions, toroidal Alfvén eigenmodes (TAEs) [3] have been observed to cause a loss of over 50% of the injected beam power leading to a significant ablation of plasma facing components [4]. In realistic 3D configurations with magnetic field ripple such as that produced by the toroidal field coils, TAE induced energetic particle transport has been observed to cause, under certain conditions, severe damage of the vacuum vessel leading to machine venting [5]. Future burning plasmas with a large population of super-Alfvénic alpha particles are prone to develop Alfvén perturbations that, if not mitigated, can lead to unacceptable consequences. Alfvén eigenmode (AE) mitigation techniques based on external, and controlled, actuators are therefore mandatory. Based on the main AE drive and damping mechanisms, several control techniques have been successfully explored during the last years [6, 7] though their applicability to future devices is still under investigation.

This paper gives an overview of the main control techniques that have proven to work in present devices together with our current understanding and their prospects towards future devices such as ITER. After a first introduction on the need of the development of reliable external actuators to control AEs in burning plasmas, the basic AE physics needed to develop control techniques in toroidal devices are summarized in section 2. Section 3 is devoted to the energetic particle drive. In section 4, the main AE control techniques in present devices are discussed. The last section is devoted to a discussion on the prospects that these techniques have in future burning plasmas.

2. Alfvén waves in toroidal devices

Shear (torsional) Alfvén waves are transverse, low frequency (compared to the ion cyclotron frequency) electromagnetic waves that propagates along the magnetic field, **B** [8, 9]. In the absence of kinetic effects, magnetic field lines and ions oscillate, in a uniform field, with a dispersion relation given by:

$$\omega = k_{||} v_A,$$

where $k_{||}$ is the wave vector parallel to the magnetic field and

$$vA = \frac{B}{\sqrt{\mu_0 \sum n_i m_i}}$$

is the Alfvén speed. Here μ_0, is the vacuum magnetic permeability and $\sum n_i m_i$ is the plasma mass density.

Quasi-neutral plasmas that are dominated by species with a similar charge/mass ratio have a mass density that is linearly proportional to the electron density, n_e, and thus $v_A \propto \frac{B}{\sqrt{ne}}$. Shear Alfvén waves are transverse polarized waves with perturbation electric and magnetic fields oscillating mainly in the perpendicular direction to the wave propagation, i.e. $\tilde{E}_{||} \ll \tilde{E}_{\perp}$ and $\tilde{B}_{||} \ll \tilde{B}_{\perp}$. Shear Alfvén waves are similar to transverse waves on a guitar, the tension is provided by the magnetic field and the mass density by the ions.

In a toroidal geometry, due to the toroidal and poloidal periodicity constraints, a wave field perturbation, i.e. fluid displacement in ideal MHD, may be described by a Fourier decomposition in poloidal and toroidal harmonics. The fluid displacement vector can, thus, be described as

$$\xi(r, \varphi, \theta) = \sum_{m,n} \xi_{m,n}(r) \mathrm{e}^{\mathrm{i}(n\varphi - m\theta - \omega t)},$$

where n and m are the mode numbers in the toroidal and poloidal direction respectively. In a toroidal axisymmetric device with circular cross-section, the equilibrium magnetic field $B = B_0\left(1 - \frac{r}{R_0}\cos\theta\right)$ is a function of r and θ and thus the magnetic field lines form helixes around the magnetic axis. In tokamaks, the 'twist' of the magnetic field lines, B, as a function of the minor radius, r, is determined by the safety

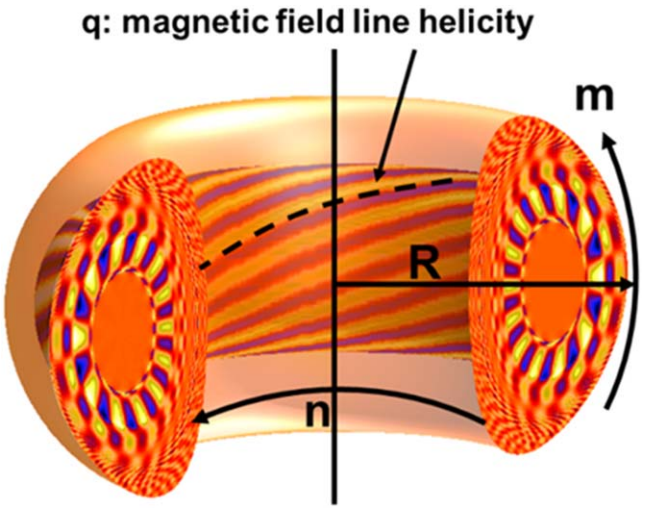

Figure 1. ITER. Simulated toroidally induced Alfvén eigenmode (TAE) structure in ITER. The major radius, R, safety factor, q, and the toroidal and poloidal mode numbers are indicated with their helical symmetry direction.

factor

$$q(r) \equiv \boldsymbol{B} \cdot \nabla\varphi / \mathbf{B} \cdot \nabla\theta,$$

where r is constant on a magnetic flux surface, and (φ, θ) are the appropriate toroidal and poloidal angle coordinates. Figure 1 shows the relevant parameters for this Fourier decomposition with the tokamak helical structures. This helical periodicity requires that $k_{||} = (nq - m)/qR$ and, as the safety factor, q, is a function of r, the dispersion relation $\omega = k_{||}(r)v_A$ is also a function of r. This dispersion relation forms the Alfvén *continuum* [10] in a non-uniform plasma with all possible Alfvénic frequencies allowed to exist as local (radial) singular oscillations [11]. The continuous spectrum decays algebraically in time due to phase mixing [10], while a test wave is absorbed at the radial position where it resonantly excites the shear Alfvén *continuum* [12, 13]. The Alfvén *continuum* damping rate is given by the gradient of frequency of local (radial) singular oscillations, $\gamma \sim \frac{\mathrm{d}(k_{||}v_A)}{\mathrm{d}r}$ (see [14] and references therein).

The existence of periodic magnetic mirrors along field lines in toroidal devices with rotational transform, and $B \propto R^{-1}$, creates gaps in the Alfvén *continuum* where a discrete spectrum of Alfvén waves may exist. These discrete spectrum waves, AEs, do not experience significant continuum damping effect, and can thus be easily excited by the energetic particles.

Periodic variations in the magnetic field or plasma mass density leads to periodic variations in the Alfvén speed and ultimately in the index of refraction. A periodic variation in the index of refraction leads to a band gap centre at the Bragg frequency:

$$f = \frac{\bar{v}}{2\Delta z},$$

where $\bar{v}$ is the average phase velocity and Δz is the distance between the periodic varying elements. In a torus, the poloidal distance around the torus for a field line is given by

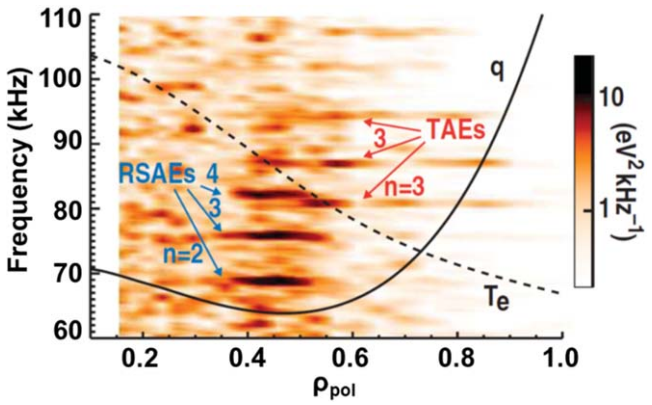

Figure 2. DIII-D. Measured radial profile of electron temperature fluctuations at the DIII-D tokamak. The q-profile and electron temperature profile, T_e, are overplotted in black with solid and dashed lines respectively. Reprinted figure with permission from [19], Copyright 2006 by the American Physical Society.

$\Delta z = q2\pi R$, and so the TAE gap is centred at

$$f = \frac{v_A}{2(q2\pi R)} = \frac{v_A}{4\pi qR}.$$

The width of the gap depends on the variation in field strength, $\frac{B_{\max}}{B_{\min}} \propto 1 + \frac{2r}{R}$, and so the gap width which is proportional to $\frac{\Delta B}{\bar{B}}$ is proportional to the machine inverse aspect ratio $\epsilon = r/R$ where r is the plasma minor radius.

The two most deleterious AEs in a toroidal device are reversed shear Alfvén eigenmodes (RSAEs) [15] and TAEs [16–18]. RSAEs occur in plasmas with a minimum in q-profile where $\frac{\mathrm{d}(k_{||}v_A)}{\mathrm{d}r} = 0$ and thus the wave is trapped in an effective potential well. RSAEs are characterized by a single dominant poloidal harmonic m and, as $q_{\min}$ decreases from m/n to $(m - 1/2)/n$, an additional harmonic $m - 1$ grows in amplitude until the mode becomes a TAE. The RSAE frequency tracks the evolution of $q_{\min}(t)$ following the expression

$$f_{\mathrm{RSAE}} = \left| \frac{m}{q_{\min}(t)} - n \right| \frac{v_{\mathrm{A}}}{2\pi \mathrm{R}_0} + \Delta f,$$

where Δf includes effects associated with thermal plasma pressure and pressure gradients as well as the energetic particle response. The RSAE frequencies lie in the frequency band between the geodesic acoustic mode (GAM) and the TAE frequencies with

$$f_{\mathrm{GAM}} \cong \frac{1}{2\pi}\left[\frac{2}{m_i \mathrm{R}}\left(T_e + \frac{7}{4}T_i\right)\right]^{1/2} < f_{\mathrm{RSAE}} < f_{\mathrm{TAE}}.$$

TAE gaps appear at the frequency crossing between two waves with m and $m + 1$ poloidal mode numbers with the same toroidal mode number, n. The frequencies of the continuum modes cross at the radius where the parallel wave number have the same absolute value and form a TAE when radial non-uniformity and equilibrium geometry provide an effective potential well for a bound state to exist [6, 14].

Weakly damped modes such as RSAEs and TAEs are commonly destabilized by energetic particles in toroidal devices. Figure 2 shows the measured profile of the electron

temperature perturbation as a function of frequency and plasma minor radius in the DIII-D tokamak [19]. RSAEs are clearly visible at $q_{\min}$ while TAEs are radially extended and exist at higher frequencies. In ITER DT burning plasmas, Alfvén waves will be well decoupled from the thermal plasma with $v_{\mathrm{th},i} \ll v_A \ll v_{\mathrm{tch},e}$ and are thus, likely to be weakly damped (here, $v_{\mathrm{th},i}$ and $v_{\mathrm{th},e}$ are the ion and electron thermal velocities respectively) and excited.

3. Instability drive by energetic particles

In toroidal devices, AEs are typically driven unstable by gradients in an energetic particle distribution that fulfil a resonant condition given by the wave dispersion relation, $\omega = k_{||} \cdot v_A$, and particle orbital frequencies. For trapped particles, the resonance condition can be written as $\omega = n \cdot \omega_p + p \cdot \omega_b$, where n is the toroidal mode number, ω_p is the toroidal precession frequency, ω_b is the poloidal bounce frequency and $p = 0, \pm 1, \pm 2 \ldots$ the relevant resonance poloidal harmonic. The energetic particle drive, $\gamma_{\mathrm{EP}}^{\mathrm{drive}}$ must overcome the sum of all possible damping mechanisms which are mostly given by the Alfvén *continuum* and thermal plasma kinetic effects [20–24]. The energetic particle drive is proportional to the energetic particle pressure, β_{EP}, as well as to gradients in the energetic particle spatial and energy distribution following the expression

$$\frac{\gamma_{\mathrm{EP}}^{\mathrm{drive}}}{\omega} \propto \beta_{\mathrm{EP}} \left(\frac{n}{\omega} \frac{E}{f} \frac{\mathrm{d}f}{\mathrm{d}P_\varphi} + \frac{E}{f} \frac{\mathrm{d}f}{\mathrm{d}E} \right).$$

Here n and ω are the AE toroidal mode number and frequency and f, E and P_φ are the particle distribution, energy and toroidal canonical angular momentum respectively. The particle canonical angular momentum, P_φ, is given by

$$P_\varphi = mRv_\varphi - Ze\Psi_p.$$

With m, R, v_φ and Ze the particle mass, radial position, toroidal velocity and charge and Ψ_p the poloidal magnetic flux at the particle position. This expression relates unequivocally the particle's radial position with its canonical angular momentum, P_φ, and thus, momentum and radial gradients in the particle distribution are analogous. In the presence of a perturbation with a single toroidal mode number, n, and frequency ω, a variation in the particle energy leads to a variation in its canonical angular momentum following the expression [25]

$$\frac{\mathrm{d}P_\varphi}{\mathrm{d}t} = \frac{n}{\omega} \frac{\mathrm{d}E}{\mathrm{d}t}.$$

Wave–particle energy exchange implies a particle transport that modifies the distribution radial gradients and thus, the energetic particle drive.

The second term in the energetic particle drive expression indicates whether the energetic particle distribution damps the wave via Landau damping or drives it unstable via inverse Landau damping.

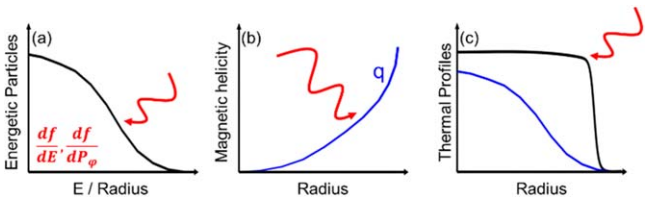

Figure 3. Cartoon of control variables for AE activity in present devices. Red arrow indicates external actuator.

4. AE active control techniques

Present fusion devices are equipped with a broad set of external actuators that allow modification of AE activity by acting directly on their drive, i.e. energetic particle distribution, damping mechanisms, i.e. Alfvén *continuum* or thermal kinetic effects or eigenmode existance. Figure 3 shows a cartoon of the control variables that can be modified externally in present devices to change the AE activity. While a modification in the gradients of the energetic particle distribution will affect directly the wave drive, a modification in the magnetic helicity will predominantly affect the eigenmode existence and Alfvén *continuum*, i.e. *continuum* damping. A modification in the thermal kinetic profiles, e.g. electron density, n_e and electron temperature, T_e, leads to a change in the wave drive and damping rates. In general, all these control variables are closely linked to each other and a modification in one of them typically leads to a modification in some of the others, e.g. a modification in the q-profile changes the Alfvén *continuum* and thus, the *continuum* damping but also the energetic particle distribution and thus, the wave drive. In the following, a survey of the most successful and promising control techniques in present tokamaks and stellarators is presented.

4.1. Toroidally asymmetric radio frequency waves

In tokamaks, in the presence of ICRF waves, neither the particle energy, E, nor the toroidal angular momentum, P_φ, are conserved. However, their combination, $E - \left(\frac{\omega}{n}\right)P_\varphi$, is conserved. Here ω is the ICRF frequency, and n is toroidal mode number of the ICRF wave. This conservation law gives, as shown in the previous section, $\Delta P_\varphi = \left(\frac{n}{\omega}\right)\Delta E$, so that the average increase in the energy of ICRF-heated ions, $\Delta E > 0$, leads to a drift in the positive or negative direction of P_φ depending on the sign of n [26–28]. Experiments on the JET tokamak have shown that the ^{3}He energetic particle profile can be modified by launching ICRF waves with different n-signs [28]. Direct evidence for the wave-induced particle pinch was obtained from measured γ-ray emission profiles. Energetic particle peaked profiles were observed with $+90°$ ICRF waves while flatten profiles were obtained with $-90°$ ICRF waves. Figure 4 shows the measured γ-ray emission profiles with these two ICRF wave configurations. Concurrent differences in the AE activity were observed with different fast-ion gradients. High harmonic fast waves have also been

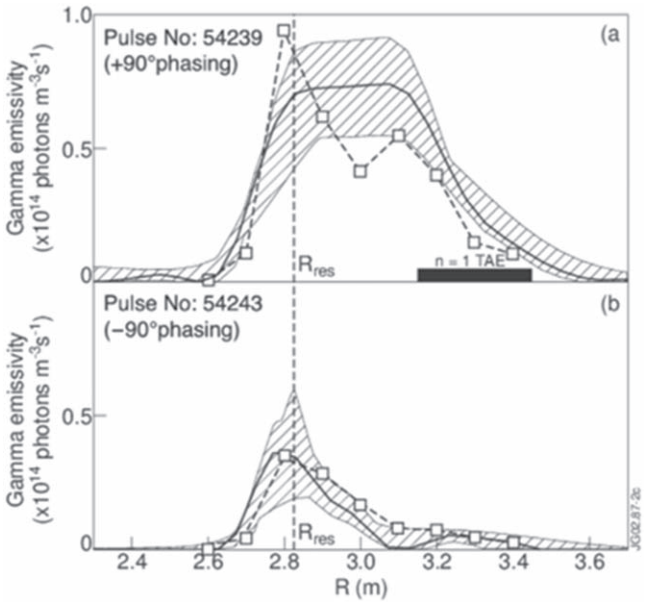

Figure 4. JET. Reconstructed local gamma-ray emissivity (solid lines) together with the calculated gamma-ray emissivity along the mid-plane. The localization of observed $n = 1$ TAE is indicated in (a). Reprinted figure with permission from [28], Copyright 2002 by the American Physical Society.

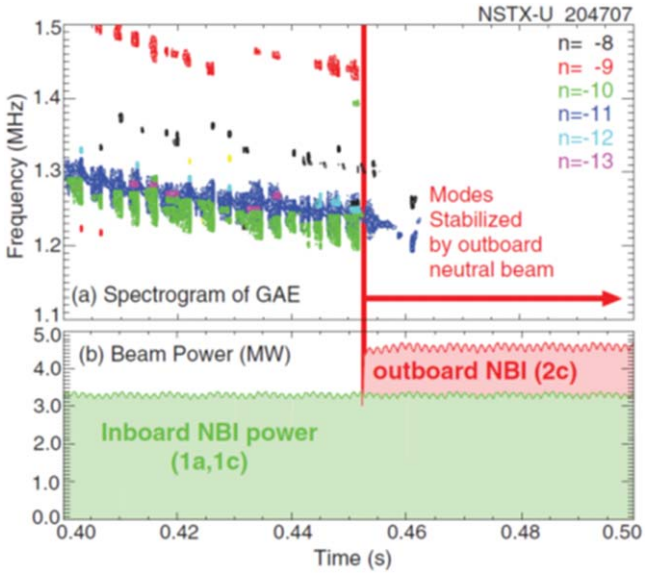

Figure 5. NSTX. (a) Magnetic spectrogram showing counter-propagating GAE activity. (b) Beam power of on-axis (green) and off-axis (red) NBI sources. Reprinted figure with permission from [33], Copyright 2017 by the American Physical Society.

successfully used to suppress TAEs in the NSTX tokamak by modifying the fast-ion distribution in phase-space [29].

4.2. Variable NBI

In contrast to the fusion born alpha particle distributions, the energetic particle distributions generated by external heating systems such as ICRH or NBI are highly anisotropic. The capability to control the operation parameters of the external heating systems can be used to modify the energetic particle population and so change gradients and populate or depopulate the wave–particle resonances responsible for the AE drive. Extensive effort is being put toward modifying AE activity via variable NBI heating power, and torque [30], toroidal rotation shear [31], the energy and pitch-angle of the injected particles [32, 33] and the spatial gradients of the fast-ion distribution [34, 35]. Recent experiments at NSTX exploited these capabilities with in- and out-board NBI heating. While in-board heating is typically used in NSTX to excite global Alfvén eigenmodes (GAE) unstable, outboard NBI sources are observed to stabilize them [33]. Figure 5 shows the experimental suppression of GAEs through off-axis NBI heating. The Doppler-shifted ion cyclotron resonance model predicts that for $k_{\mathrm{perp}}\rho_L < 1.9$, the resonant fast-ions will be stabilizing, and destabilizing for $1.9 < k_{\mathrm{perp}}\rho_L < 3.9$, where ρ_L is the Larmor radius. The experimental results, hybrid kinetic-MHD simulations carried out with the HYM code [36] and analytic theory all suggest that stabilization is due to an increase in the population of low pitch, deeply passing particles with small Larmor radius.

4.3. Localized electron cyclotron resonance heating

Local changes in thermal plasma profiles induced by localized ECRH could have a major impact on the Alfvénic stability modifying their drive and/or damping. As seen in the previous section, AEs are, indeed, extremely sensitive to the safety factor, q, and thermal density, n_e, and temperature, T_e profiles. Recent experiments in the AUG and DIII-D tokamaks have shown the profound effect that localized ECRH has on the observed AE activity. In early NBI heated discharges with elevated and reversed q-profiles, localized ECRH has been observed to mitigate [37] or even suppress RSAEs [38, 39]. Systematic shot-to-shot radial scans in the ECRH power deposition location has allowed to investigate the impact that localized ECRH has on the observed RSAE activity when the power is deposited near the plasma centre, at the q_{min} position, or at the outer mid-plasma radius. Figure 6 shows the DIII-D poloidal cross-section and safety factor $q(r)$ in the representative reconstructed equilibria with NBI and ECRH applied shot-to-shot from the plasma centre (position P1) to outside the q_{min} surface (position P5). In discharges with on-axis ECRH (1.9 MW), a rich pattern of AE fluctuations was observed while much weaker AE activity with RSAEs almost suppressed is observed when ECRH is applied at q_{min}, see figure 7. In agreement with DIII-D results, in similar experiments at AUG a complete RSAE suppression when ECRH is applied at the q_{min} location was observed. Figure 8 shows the AE induced electron temperature fluctuations measured with the electron cyclotron emission (ECE) system in the AUG discharge near q_{min} with the ECRH power deposited near the magnetic axis (a) and near q_{min} (b).

The observed modification of RSAE activity by ECRH in AUG and DIII-D discharges is net result of several combined effects, a thorough understanding of which is complicated by

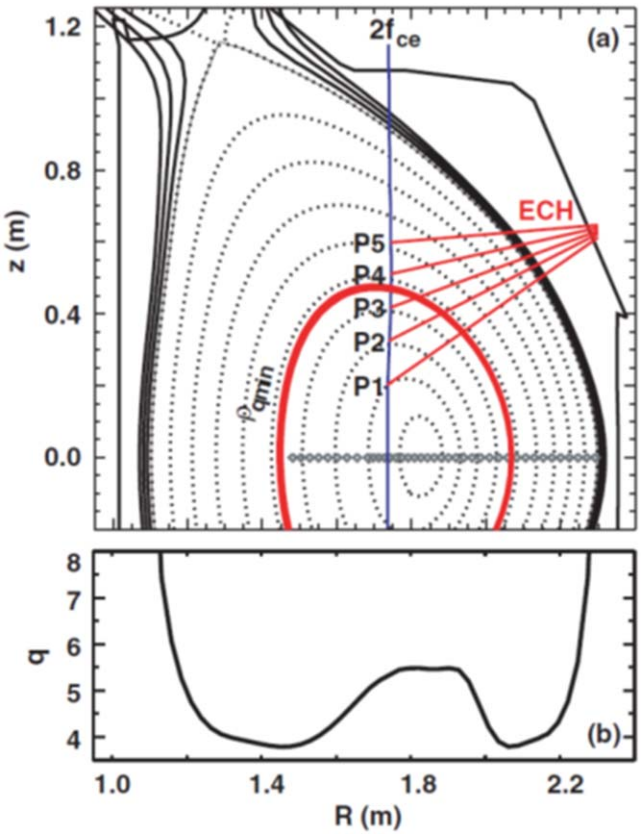

Figure 6. DIII-D. (a) Equilibrium for reversed-shear discharges with NBI and ECRH applied at positions P1-P5. The position of $q_{\min}$ is shown in red. (b) q-profile. Reproduced from [37]. © IOP Publishing Ltd. All rights reserved.

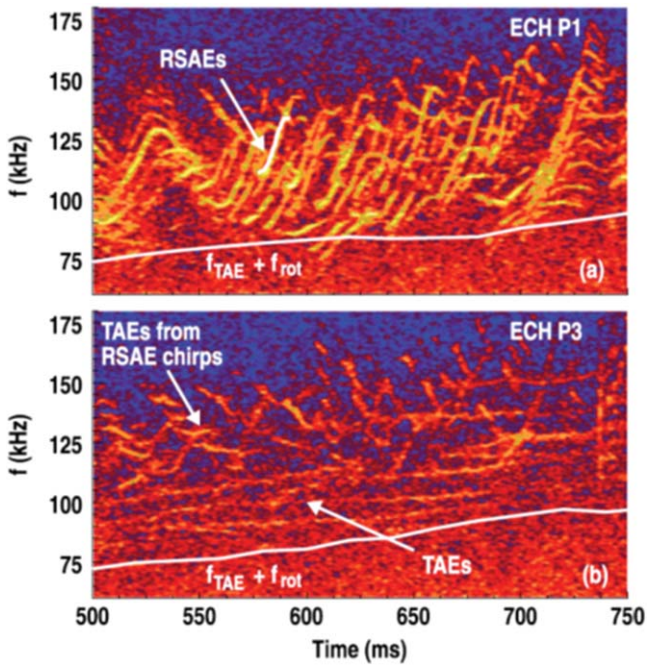

Figure 7. DIII-D. AE density fluctuations as measured by interferometry with (a) ECRH on-axis and (b) ECRH at $q_{\min}$ Reproduced from [37]. © IOP Publishing Ltd. All rights reserved.

the fact that localized electron heating impacts essentially all aspects of AEs, including mode drive, damping, and the ideal eigenmode itself. Mode stability is altered through modification of the different damping channels (electron collisional [40] and electron Landau [41] in particular, and even continuum damping [42] through pressure or rotation [31, 43] induced changes to the modes and continuum), mode drive (T_e directly impacts electron drag on fast ions), and the AEs themselves through coupling to sound waves via changes to T_e/T_i [44]. Recent predictions also indicate AE saturation and their impact on the fast-ion profile can be affected by microturbulence [45] which can be modified by ECRH. Additionally, detailed theoretical analysis has shown that horizontal polarization of flux surfaces by ECRH can form a potential hill for RSAEs and can account for RSAE elimination even at relatively low ECRH power [46, 47].

Recent DIII-D experiments utilized a simplified oval geometry and, in addition to ECH injection location, included variations of current ramp rate, ECH injection timing, and neutral beam power to try to unravel the dominant factors responsible for the change in RSAE activity [48]. Essentially all variations carried out in the experiment were observed to change the impact of ECRH on AE activity significantly. In some cases, RSAEs were observed to be more unstable with ECH near $q_{\min}$ as opposed to near the magnetic axis, in contrast to the original experiments. A consistent finding in that work was a large role of the local electron temperature profile and its gradients. The presence of frequency sweeping RSAEs was found to strongly depend on the ratio of the RSAE minimum frequency (which includes an upshift from the local GAM frequency at $q_{\min}$ by an amount dependent on gradients in the local pressure) to the TAE frequency—when the two become comparable, no frequency sweeping RSAEs are observed and only TAEs remain. More detailed calculations showed the typical frequency sweeping RSAE is very sensitive to finite pressure effects, particularly gradients in plasma pressure, and was no longer an eigenmode of the system. A similar effect may occur in the AUG experiments shown in figure 8. In that case, only low energy ~60 keV beams were used and it is conjectured that TAEs could not be driven effectively—this idea is supported by the lack of TAEs in both figures 8(a) and (b). It is pointed out that while finite pressure effects can explain a large fraction of the observations in [48], it cannot account for all observations of the impact of ECRH on beam driven AEs in AUG and DIII-D. Examples where additional factors are obviously important are the rapid modulation of TAEs observed during modulated ECRH in [49] as well as a persistent lack of RSAE even after T_e profiles have relaxed to those supporting RSAE in different discharges [50].

The use of localized ECRH is an important and unique area of AE control research since individual modes can be specifically targeted and, as pointed out above, there are many different avenues for the interaction to take place. A promising direction for future experiments is the use electron cyclotron current drive to locally modify magnetic shear and alter AE damping. Additionally, the idea of flux surface polarization and its impact on AEs is an interesting concept

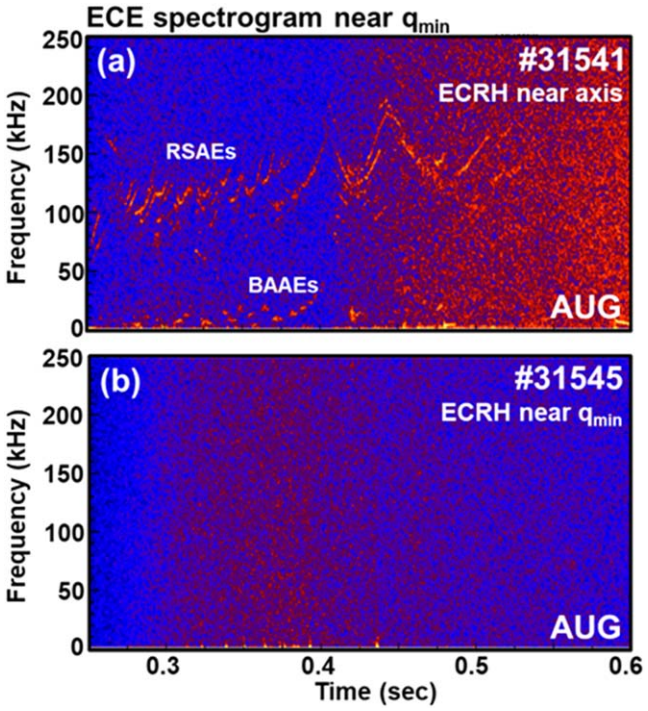

Figure 8. AUG. AE local temperature fluctuations measured with the electron cyclotron emission (ECE) system at the q_{min} location [38, 39]. Reproduced from [39]. © 2017 CCFE.

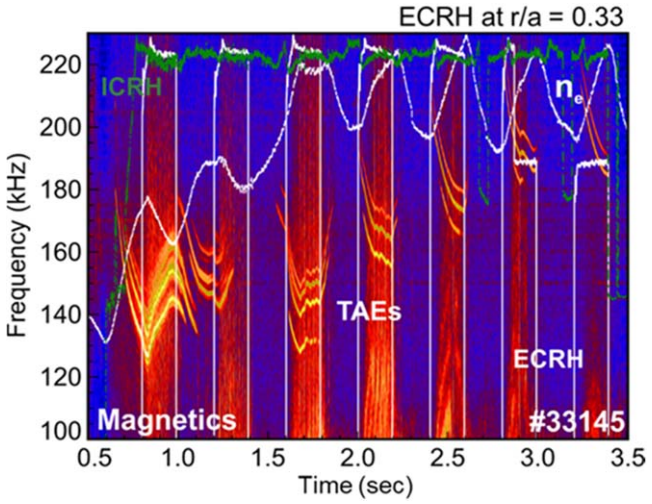

Figure 9. AUG. Magnetic spectrogram showing TAE fluctuations. The ICRH and ECRH heating powers are highlighted in green and white respectively. The temporal evolution of the core line integrated density is also depicted in white. Reproduced from [39]. © 2017 CCFE.

that deserves investigation. Since the effect depends on distortion of the electron distribution function, RSAE suppression should persist for timescales similar to the electron-electron collision time. Hence, investigation of the AE response due to ECRH modulation, like that presented in [49], as well as wave polarization is warranted.

In NBI heated plasmas, the impact of localized ECRH on TAEs is not as clear, instead, in ICRF heated AUG discharges, strong TAEs appear with off-axis ECRH. Figure 9 shows the AE activity as measured with a magnetic pick-up coil in ICRF heated AUG discharges with off-axis ECRH heating. The TAE occurrence is remarkably correlated with the off-axis ECRH blips with a time response on the order of a few ms. At the beginning of the discharge, the low plasma density and elevated q-profile lead to a very high energetic particle content and pressure, with respect to the thermal plasma pressure and, thus, to a high energetic particle drive. Local ECRH blips are not capable of affecting significantly the observed AE activity. As the density and q-profile relax, the energetic particle drive relaxes too, TAEs get closer to marginal stability and can therefore be easily affected by local (off-axis) ECRH blips, see figure 9 from 1.5 to 3.5 s. In these experiments, off-axis ECRH heating tends to facilitate the appearance of TAEs driven unstable by supra-alfvénic ICRH ions. In contrast, on-axis ECRH does not show any impact on TAEs driven unstable by ICRH ions. Modelling suggests that localized ECRH leads to higher local electron temperatures and thus to longer fast-ion collisional times that increases the fast-ion content and gradients at the wave–particle resonances responsible for the TAE drive [39].

Experiments in fusion devices with different magnetic configurations confirm that local ECRH can have an important impact on the observed AE activity in tokamaks and stellarators. TJ-II experiments show that main AE properties can be changed radically by application of localized ECRH. Depending on the ECRH deposition location, AEs in TJ-II can go from chirping to steady frequency and higher or lower amplitude. Lower amplitude steady modes appear to occur when ECRH is deposited inside the mode location. Figure 10 shows the AE activity in a TJ-II experiment with varying ECRH timing and power. The AE activity is clearly modified by the application of ECRH [50]. Recent experiments at LHD have shown that localized ECRH can also be used to control the stability of fast-ion driven instabilities by shrinking the eigenmode making it smaller than the trapped orbit width [51].

4.4. Electron cyclotron current drive

The AE activity observed in a toroidal device with rotational transform depends strongly on the Alfvén *continuum* and associated gaps supported by the magnetic equilibrium and thermal plasma profiles [14]. In tokamaks, for example, TAEs are not supported by the background if the plasma pressure gradient exceeds a critical value given by the magnetic shear, aspect ratio, and Shafranov shift [22, 52–56]

$$\alpha \equiv -R_0 q^2 \frac{\mathrm{d}\beta}{\mathrm{d}r} > \alpha_{\mathrm{crit}} = (\epsilon + 2\Delta') + S^2,$$

where Δ' is the Shafranov shift and S the magnetic shear. The modification of the local shear through localized ECCD in tokamaks with large plasma currents is rather challenging and difficult to decouple from other side effects associated with the application of ECCD, i.e. heating. Stellarators with negligible plasma currents are excellent testbeds to test the sensitivity of the observed AE activity to local changes in the rotational transform induced by externally applied and highly

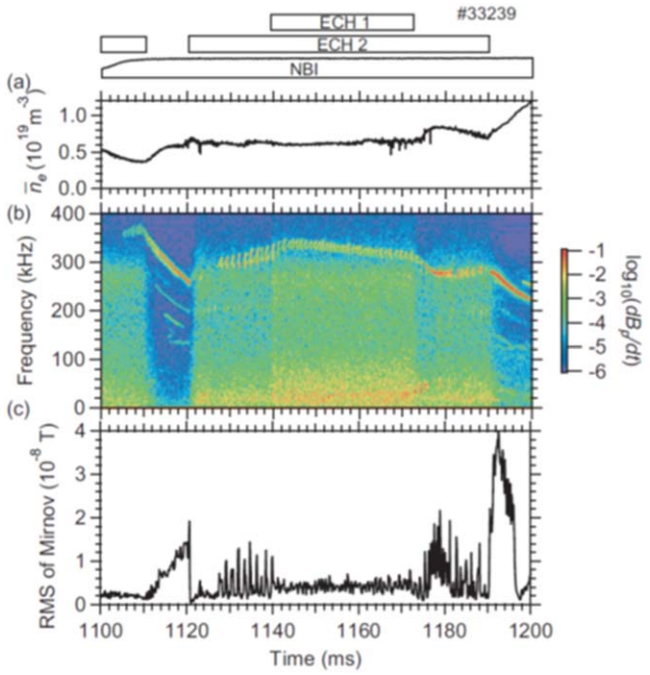

Figure 10. TJ-II. Temporal evolution of the plasma heating, density (a), magnetic spectrogram (b), and root-mean-square (RMS) of band-pass filtered magnetic fluctuation (δB) at the time varying AE frequency. Reproduced courtesy of IAEA. Figure from [50]. Copyright 2013 IAEA.

localized ECCD. In stellarators, the ECCD can, indeed be a significant part of the total plasma current maximizing the ECCD effect on the observed AE activity. Striking results are obtained in the Heliotron J where ECCD with $N_{||} = 0.15$ is observed to fully suppressed NBI driven GAEs as figure 11 shows [57].

4.5. Externally applied resonant magnetic perturbations (RMPs)

In toroidal devices, externally applied perturbative 3D fields are routinely used to improve the plasma stability against a rich spectrum of MHD fluctuations such as ELMs [58–60] or RWMs [61]. Externally applied RMPs have been recently used in NSTX to mitigate TAEs and GAEs through fast-ion redistribution in particle phase-space [62, 63]. In response to perturbations with an amplitude of $\frac{\delta B}{B} \sim 0.01$ at the plasma boundary, the mode amplitude is reduced, the mode bursting frequency is increased, and the frequency chirp is smaller. For modes of weaker bursting character, the magnetic perturbation induces a temporary transition to a saturated continuous mode. Figure 12 shows the modification of the GAE activity as RMP blips are applied to a NBI heated discharge.

The resonance condition for GAE modes is

$$\omega = k_{||} v_{||} + l\omega_{\mathrm{ic}}$$

where ω is the wave frequency, $v_{||}$ is the ion velocity component along the field line, and ω_{ic} is the ion cyclotron frequency. For the observed GAEs in NSTX, possible unstable resonances include direct $l = 0$ resonances in the core and in

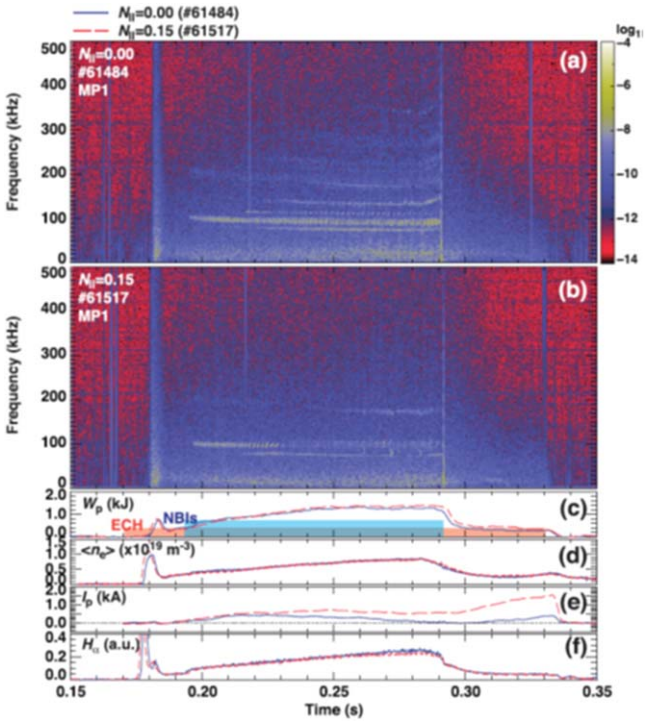

Figure 11. Heliotron J. Temporal evolution of the magnetic activity as measured by a magnetic pick-up coil in a discharge without ECCD, i.e. $N_{||} = 0$ (a) and with ECCD and $N_{||} = 0.15$ (b). Temporal evolution of plasma stored energy (c), line average electron density (d), plasma current (e), and Lyman alpha line for the case with $N_{||} = 0$ (red) and $N_{||} = 0.15$ (blue) (f). Reproduced courtesy of IAEA. Figure from [57]. Copyright 2017 IAEA.

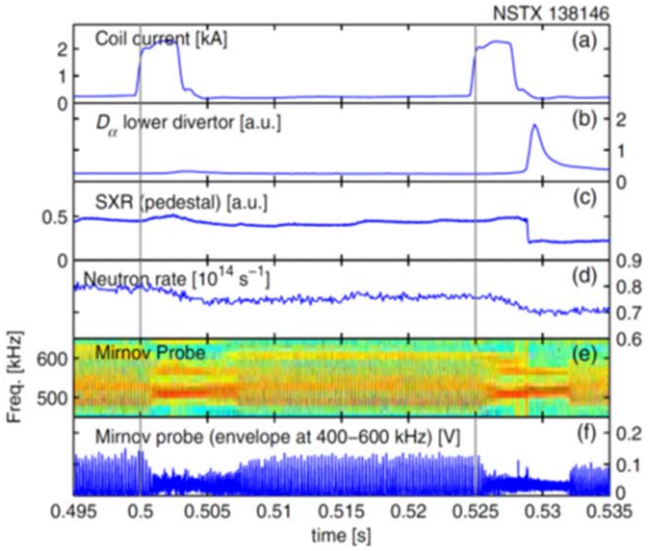

Figure 12. NSTX. AE mitigation in NSTX via externally applied 3D fields. (a) RMP coil current per turn, (b) Dα light, (c) soft x-ray emission from the plasma pedestal, (d) neutron rate, (e) spectrogram of high frequency Alfvén activity from a magnetic pick-up coil and (f) bandpass filtered magnetic pick-up coil signal. Reprinted figure with permission from [62], Copyright 2011 by the American Physical Society.

the plasma edge and a $l = 1$ Doppler-shifted cyclotron resonance in the plasma core. The RMP alters the fast-ion distribution function at several of these candidate resonances.

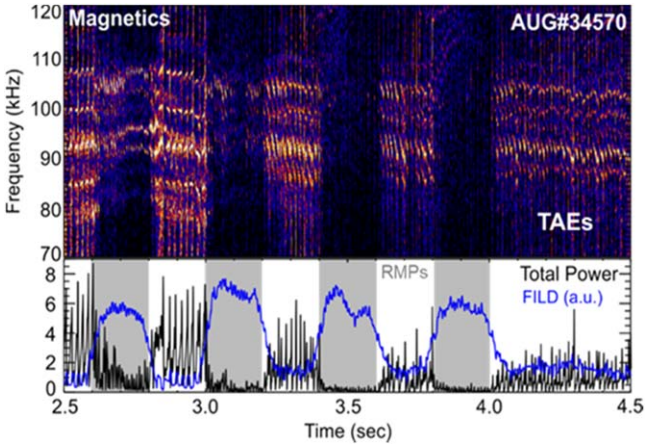

Figure 13. AUG. TAE suppression via externally applied 3D fields in the AUG tokamak. Top panel shows a magnetic spectrogram. Bottom panel shows the temporal evolution of the TAE RMS signal (black) together with the measured fast-ion losses (blue). The timing of the applied 3D fields is indicated in the bottom panel with vertical grey stripes.

Simulations of the perturbed distribution function due to the applied 3D fields including the plasma response calculated with the IPEC code [64] indicate, indeed, that the 3D perturbation affects the orbits of fast-ions that resonate with the bursting modes at several resonances.

Similar experiments have been recently carried out in the AUG tokamak with strong NBI driven TAEs. In some cases, RMPs have been observed to fully suppress TAEs in AUG discharges with elevated q-profiles. Figure 13 shows the TAE activity, with frequencies between 70 and 120 kHz, measured with a magnetic pick-up coil in these AUG experiments. A clear modulation of the TAE activity is observed with the application of the externally applied 3D fields. The timing of the applied RMPs is highlighted in the bottom panel of figure 13 with vertical grey stripes. In the bottom panel, the temporal evolution of the TAE RMS amplitude is plotted together with that of the of the measured fast-ion losses. As the discharge evolves in time, and the q-profile relaxes, the overall TAE activity becomes weaker. The RMP blips are clearly modulating the TAE activity and eventually even suppressing them completely. Fast-ion losses measured with one of the AUG fast-ion loss detectors (FILD) [65] show a clear correlation with the applied 3D fields and TAE activity indicating that the applied RMPs are probably ejecting from the plasma the fast-ions that would otherwise drive the modes unstable. The velocity-space of the measured fast-ion losses show several populations with different energies (gyroradius) and pitch-angles ($\Lambda = \arccos\frac{v_{||}}{v_{\rm tot}}$), see figure 14. Most of the losses appear at the injection energy, $\rho_L \approx 3.5$ cm, and two different pitch-angles, $\Lambda \approx 50°$ and $\Lambda \approx 65°$. Full orbit simulations have been carried out to identify the orbit topology of the measured escaping ions following them from the detector aperture all the way back to the plasma with the measured energies and pitch-angles. Figure 14(b) shows that the most intense signal is coming from barely trapped particles on wide banana orbits while the losses that appear at high pitch-angles correspond to deeply trapped orbits. Both orbits

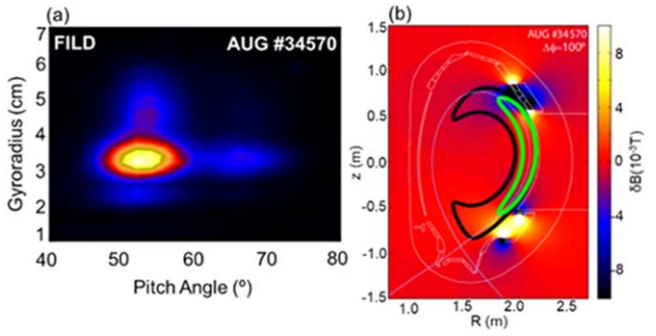

Figure 14. AUG. (a) Velocity-space of escaping ions measured with FILD. (b) Trajectories of the measured escaping ions followed backwards in time from the FILD detector aperture back to the plasma.

are exploring the entire pedestal and scrape-off layer passing close to the RMP coils (area of maximal RMP perturbation strength).

In order to understand the physical mechanism underlying the observed additional losses in the presence of externally applied 3D fields, the variation of the fast-ion canonical angular momentum, P_φ, in a 3D field perturbed equilibrium has been computed using the full orbit ASCOT code [66] for particles with the main pitch-angles observed in figure 14(a) and vacuum fields [67]. The 3D fields configuration is given by AUG RMP coils with a differential phase between the upper and lower set of RMP coils $\Delta\varphi_{\rm UL} = 40°$. Figure 15 shows the calculated δP_φ for an ensemble of particles with energies between $E = 20$ keV and $E = 100$ keV and initial radial coordinate between $R = 1.95$ m and $R = 2.20$ m and $R = 2.20$ m. The maximum negative variation of P_φ (outward transport) is localized within 5 cm around the separatrix (indicated by a vertical dashed line in figure 15) with a strong dependency on the radial coordinate but not on the particle energy.

Following [68–70], calculations of the particles orbital frequencies, i.e. poloidal bounce frequency (ω_b) and toroidal precession frequency (ω_d) [14, 71] show that the maximum in δP_φ coincides with rational values of $\frac{\omega_b}{\omega_d}$ that fulfil a geometrical nonlinear resonance condition that can be derived from a Fourier decomposition of the perturbed particle orbits in the presence of the externally applied 3D fields. A scalar function describing a nearly stationary field that changes in the poloidal and toroidal direction can be written as:

$$f(r,\,\theta,\,\phi) = \sum_{n,m} \mathrm{e}^{\mathrm{i}(n\phi - m\theta)} f_{m.n}(r,\,\theta,\,\phi)$$

in terms of the bounce averaged particle coordinates $(r,\,\theta,\,\phi)$. This field projected along the trajectory of a trapped particle takes the form:

$$f(r,\,\theta,\,\phi) = \sum_{n,m} \mathrm{e}^{\mathrm{i}(n\omega_d - p\omega_b)\tau} P_{n,m,p} \cdot f_{m.n}(r,\,\theta,\,\phi),$$

where τ is a time variable that follows the trapped particle along the bounce motion. This equation gives the linear resonance condition $n\omega_d - p\omega_b = 0$.

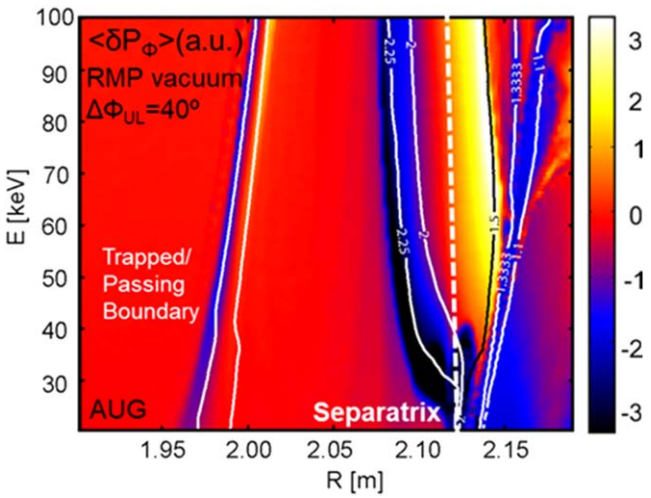

Figure 15. ASCOT. Energetic particle δP_φ induced by externally applied 3D fields with a differential phase between the upper and lower set of RMP coils $\Delta\varphi_{\mathrm{UL}} = 40^\circ$ in AUG.

If the linear condition is not satisfied and assuming that the perturbation leads to a modulation of the bounce averaged particle motion, and that this is periodic in the poloidal coordinate describing the bounce motion (i.e. the bounce-phase coordinate (θ_c)), the effect of the perturbation can be seen as a correction to the particle trajectory accumulated over one banana motion. As this correction is periodic in θ_c, the nonlinear effects of a perturbation characterized by fixed values of m, n and $p = p_0$ can be incorporated in the previous Fourier decomposition as follows:

$$f(r, \theta, \phi) \approx \sum_{p,l} \mathrm{e}^{\mathrm{i}(n\omega_d - p\omega_b)\tau} \mathrm{e}^{\mathrm{i}l(n\omega_d - p_0\omega_b)\tau} \times P_{n,m,p} \cdot f_{m.n}(r, \theta, \phi),$$

where l is the nonlinear harmonic, which is introduced when we include the nonlinear periodic correction of the particle trajectory due to the perturbation. The linear bounce harmonic $p = p_0 + p'$ contains the main bounce harmonic, which is fixed for the perodicity of perturbation, and the secondary harmonic p′ included in the bounce harmonic of the linear component. A resonant particle fulfils:

$$\frac{\mathrm{d}(\Omega\tau)}{\mathrm{d}\tau} = (n\omega_\mathrm{d} - p\omega_b) + l(n\omega_\mathrm{d} - p_0\omega_b) = 0 \rightarrow$$

And so the nonlinear resonant condition takes the form:

$$\frac{\omega_b}{\omega_d} = \frac{n(l+1)}{p_0(l+1) + p'}.$$

Looking at figure 15, nonlinear geometrical resonances seem to play a key role in the calculated δP_φ for the given 3D fields configuration as the region with the maximal δP_φ coincides with the nonlinear geometrical resonance $\frac{\omega_b}{\omega_d} = 2.25$ while the linear resonance $\frac{\omega_b}{\omega_d} = 2$ ($l = 0$) appears outside of the separatrix with overall lower δP_φ values.

5. Summary and outlook

Shear Alfvén waves are electromagnetic perturbations inherent to a magnetized plasma. In toroidal devices, shear Alfvén waves are typically strongly damped by resonant coupling with the Alfvén continuous spectrum. Poloidal asymmetries, however, can also create gaps in the Alfvén *continuum* where weakly damped AEs such as TAEs can be easily driven unstable by radial gradients in a resonant energetic particles' population. In present devices RSAEs and TAEs are observed to cause a significant redistribution and loss of energetic particles. If allowed to grow, AEs could cause a significant degradation of the fusion performance, posing even a threat to the device integrity, in a future burning plasma with a high population of super-Alfvénic alpha particles. Based on fundamental AE physics, external actuators to control the AE drive or damping are currently being developed. Most of the control techniques rely on a modification of the fast-ion distribution that is driving the AEs unstable either in geometrical or in velocity-space.

- Flexible external energetic particle sources such as ICRH or NBI are used to tailor the energetic particle population, and thus, to modify the observed Alfvénic activity. ICRH and NBI with specific heating schemes and/or geometries have been successfully used to modify energetic particles' gradients in geometrical and velocity-space and so to maximize or to minimize the wave (inverse) Landau damping. One can envisage using the ICRH and/or NBI systems in ITER to mitigate alpha particle driven AEs reversing the fast-ion population gradients at certain phase-space locations.
- Localized ECRH has been successfully used to suppress RSAEs by a frequency upshift of the *continuum* minimum that shrinks the RSAE existence frequency band between the GAM frequency and the TAE frequency to a minimum where RSAEs are not supported anymore. Although a direct modification of the Alfvén *continuum* via localized ECRH might not be feasible in ITER with an electron heating dominated by the fusion born alpha particles, localized ECRH might be useful to modify the fusion product profiles and so the Alfvén *continuum* and drive.
- A direct modification of the *continuum* damping that eventually leads to AE suppression has been made possible in stellarators by means of a change in the rotational transform that is induced by localized ECCD. In ITER, localized ECCD might be a useful tool to induce slight local q-profile modifications that can have a significant impact on the overall AE activity.
- Recently, externally applied 3D fields have been successfully used to mitigate or even suppress AEs by a modification of the energetic particle population in particles' phase-space. External coils with flexible configurations can be used to produce 3D perturbations that act on different energetic particles' populations depending

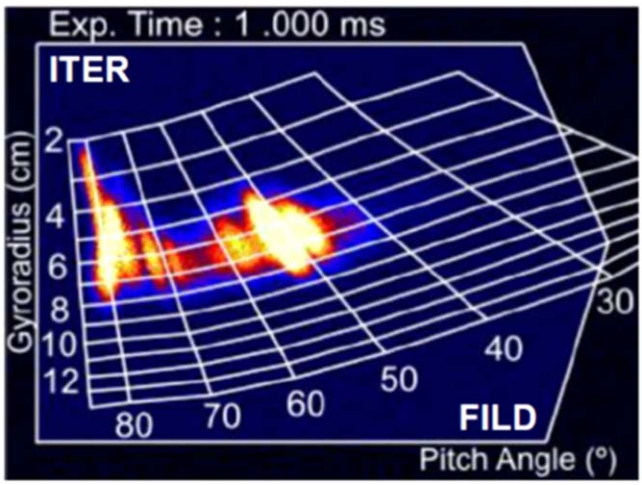

Figure 16. ITER. Synthetic FILD signal due to alpha particle losses induced by an $n = 4$ RMP. Alpha particle losses have been calculated with the ASCOT code using vacuum fields and maximal coils design currents. Reprinted figure with permission from [72], Copyright 2012 by the American Physical Society.

on the applied perturbation spectra. In ITER, the flexible RMP coils system may allow for an optimization of the applied perturbation that successfully keep ELMs under control with a tuneable energetic particle distribution and associated AE activity. Preliminary simulations of alpha particle losses induced by externally applied $n = 4$ RMPs in ITER indicate that a significant number of geometrical resonances might be present in the alpha particle population and could thus be used to their manipulation. Figure 16 shows the synthetic signal of a FILD system in ITER in the presence of alpha particle losses induced by externally applied 3D fields with $n = 4$. Several pitch-angle structures at approximately the alpha particle fusion born energy, i.e. $\rho_L \approx 6$–7 cm emerge when the 3D fields are applied [72].

- In addition to the actuators described in this paper, pellet injection or supersonic molecular beam injection that lead to rapid changes in the local thermal kinetic profiles might also be useful for AE control. Due to the density dependence in v_A, a variation in the density affects the wave–particle resonances and may cause a number of linear and nonlinear effects. Recent exploratory experiments have shown that pellet injection can, indeed, lead to a (i) AE frequency down-sweep, (ii) AE amplitude change, and (iii) spectral broadening of the observed AE toroidal mode numbers [73].

The active control of the fast-ion distribution and associated AE activity is an incipient field of research that can help optimize the performance of a future burning plasma with several external actuators working in real-time. This is, however, a quite unexplored field with just some recent attempts [74] that still requires extensive theoretical and experimental efforts.

Acknowledgments

This work has been carried out within the framework of the EUROfusion Consortium and has received funding from the Euratom research and training programme 2014–2018 and 2019–2020 under grant agreement No 633053. The views and opinions expressed herein do not necessarily reflect those of the European Commission. Support by US DOE and ITER-CN is also acknowledged. The support from the FP7 People: Marie-Curie Actions (Grant No. 321455) and the Spanish Ministry of Economy and Competitiveness (Grants No. RYC-2011-09152, No. FIS2015-69362-P) is gratefully acknowledged. The work of AVM was funded by the Russian Science Foundation, project 14-22-00193, and was partly supported by the Competitiveness Program of NRNU MEPhI.

ORCID iDs

M Garcia-Munoz https://orcid.org/0000-0002-3241-502X
J Galdon-Quiroga https://orcid.org/0000-0002-7415-1894
W W Heidbrink https://orcid.org/0000-0002-6942-8043
A V Melnikov https://orcid.org/0000-0001-6878-7493
L Sanchis-Sanchez https://orcid.org/0000-0001-8211-3356
Y Todo https://orcid.org/0000-0001-9323-8285
P Vallejos https://orcid.org/0000-0003-4343-6325
F Zonca https://orcid.org/0000-0002-9270-4704

References

[1] Fasoli A *et al* 2007 *Nucl. Fusion* **47** S264
[2] Alfvén H 1942 *Nature* **150** 405
[3] Cheng C Z, Chen L and Chance M S 1985 *Ann. Phys.* **161** 21
[4] Duong H H *et al* 1993 *Nucl. Fusion* **33** 749
[5] White R B *et al* 1995 *Phys. Plasmas* **2** 2871
[6] Herrmann M C and Fisch N J 1997 *Phys. Rev. Lett.* **79** 1495
[7] Graves J P *et al* 2012 *Nat. Commun.* **3** 624
[8] Chen L and Zonca F 2007 *Nucl. Fusion* **47** S727
[9] Heidbrink W W 2008 *Phys. Plasmas* **15** 055501
[10] Grad H 1969 *Phys. Today* **22** 34
[11] Chen L and Zonca F 1995 *Phys. Scr.* **T60** 81
[12] Chen L and Hasegawa A 1974 *Phys. Fluids* **17** 1399
[13] Chen L and Hasegawa A 1974 *J. Geophys. Res.* **79** 1024
[14] Chen L and Zonca F 2016 *Rev. Mod. Phys.* **88** 015008
[15] Sharapov S E 2002 *Phys. Plasmas* **9** 2027
[16] Heidbrink W W *et al* 2007 *Phys. Rev. Lett.* **99** 245002
[17] Garcia-Munoz M *et al* 2008 *Phys. Rev. Lett.* **100** 055005
[18] Garcia-Munoz M *et al* 2010 *Phys. Rev. Lett.* **104** 185002
[19] Van Zeeland M A *et al* 2006 *Phys. Rev. Lett.* **97** 135001
[20] Fu G Y and Van Dam J W 1989 *Phys. Fluids* **B1** 1949
[21] Betti R *et al* 1992 *Phys. Fluids* **B4** 1465
[22] Zonca F and Chen L 1992 *Phys. Rev. Lett.* **68** 592
[23] Rosenbluth M N *et al* 1992 *Phys. Rev. Lett.* **68** 596
[24] Mett R R and Mahajan S M 1992 *Phys. Fluids* **B4** 2885
[25] Chen L, Vaclavik J and Hammett G W 1988 *Nucl. Fusion* **28** 389
[26] Eriksson L G *et al* 1998 *Phys. Rev. Lett.* **81** 1231
[27] Sharapov S E *et al* 2000 *Nucl. Fusion* **40** 1363
[28] Mantsinen M *et al* 2002 *Phys. Rev. Lett.* **89** 115004

[29] Heidbrink W W *et al* 2006 *Plasma Phys. Control. Fusion* **48** 1347
[30] Pace D C *et al* 2017 *Nucl. Fusion* **57** 014001
[31] Podesta M *et al* 2010 *Phys. Plasmas* **17** 122501
[32] Fredrickson E D *et al* 2015 *Nucl. Fusion* **55** 013012
[33] Fredrickson E D *et al* 2017 *Phys. Rev. Lett.* **118** 265001
[34] Heidbrink W W *et al* 2013 *Nucl. Fusion* **53** 093006
[35] Turnyanskiy M *et al* 2013 *Nucl. Fusion* **53** 053016
[36] Belova E V, Gorelenkov N N and Cheng C Z 2003 *Phys. Plasmas* **10** 3240
[37] Van Zeeland M A *et al* 2008 *Plasma Phys. Control. Fusion* **50** 035009
[38] Garcia-Munoz M *et al* 2015 *IAEA TM on Energetic Particles in Magnetic Confinement Systems (IAEA HQ, Vienna, 4–7 September)*
[39] Sharapov S E *et al* 2018 *Plasma Phys. Control. Fusion* **60** 014026
[40] Gorelenkov N N and Sharapov S E 1992 *Phys. Scr.* **45** 163
[41] Candy J 1996 *Plasma Phys. Control. Fusion* **38** 795
[42] Berk H L, Van Dam J W, Guo Z and Lindberg D M 1992 *Phys. Fluids* B **4** 1806
[43] Saigusa M *et al* 1997 *Nucl. Fusion* **37** 1559
[44] Chu M S *et al* 1992 *Phys. Fluids* B **4** 3713
[45] Bass E M and Waltz R E 2010 *Phys. Plasmas* **17** 112319
[46] Hsu J Y *et al* 1984 *Phys. Rev. Lett.* **53** 564
[47] Marchenko V S and Bashenko O S 2013 *Plasma Phys. Control. Fusion* **55** 052002
[48] Van Zeeland M A *et al* 2016 *Nucl. Fusion* **56** 112007
[49] Van Zeeland M A *et al* 2009 *Nucl. Fusion* **49** 065003
[50] Nagaoka K *et al* 2013 *Nucl. Fusion* **53** 072004
[51] Du X D *et al* 2017 *Phys. Rev. Lett.* **118** 125001
[52] Chen L 1988 *Theory of Fusion Plasmas* ed J Vaclavik, F Troyon and E Sindoni (Bologna: Societa Italiana di Fisica/Editrice Compositor) p 327
[53] Zonca F and Chen L 1993 *Phys. Fluids* B **5** 3668
[54] Fu G Y *et al* 1995 *Phys. Plasmas*
[55] Berk H L *et al* 1995 *Phys. Plasmas*
[56] Sharapov S E *et al* 1999 *Nucl. Fusion*
[57] Yamamoto S *et al* 2017 *Nucl. Fusion* **57** 126065
[58] Evans T E *et al* 2006 *Nat. Phys.* **2** 419
[59] Loarte A *et al* 2006 *Nat. Phys.* **2** 369
[60] Suttrop W *et al* 2011 *Phys. Rev. Lett.* **106** 225004
[61] Sabbagh S A *et al* 2006 *Phys. Rev. Lett.* **97** 045004
[62] Bortolon A 2013 *Phys. Rev. Lett.* **110** 265008
[63] Kramer G J *et al* 2016 *Plasma Phys. Control. Fusion* **58** 085003
[64] Park J K, Boozer A H and Glasser A H 2007 *Phys. Plasmas* **14** 052110
[65] Garcia-Munoz M *et al* 2009 *Rev. Sci. Instrum.* **80** 053503
[66] Hirvijoki E *et al* 2014 *Comput. Phys. Commun.* **185** 1310
[67] Sanchis L *et al* 2019 *Plasma Phys. Control. Fusion* **61** 014038
[68] Chen L, Lin Z and White R 2001 *Phys. Plasmas* **8** 4713
[69] White R B, Chen L and Lin Z 2002 *Phys. Plasmas* **9** 1890
[70] Kramer G J *et al* 2012 *Phys. Rev. Lett.* **109** 035003
[71] Zonca F *et al* 2015 *New J. Phys.* **17** 13052
[72] Garcia-Munoz M *et al* 2016 *Rev. Sci. Instrum.* **87** 11D829
[73] Sharapov S E *et al* 2018 *Nucl. Fusion* **58** 082008
[74] Wenhui H *et al* 2018 *Nucl. Fusion* **58** 124001